

PuJun Wang · WanZhu Liu · ShuXue Wang  
WeiHei Song

## **$^{40}\text{Ar}/^{39}\text{Ar}$ and K/Ar dating on the volcanic rocks in the Songliao basin, NE China: constraints on stratigraphy and basin dynamics**

Received: 12 September 2000 / Accepted: 14 May 2001 / Published online: 26 September 2001  
© Springer-Verlag 2001

**Abstract** Precise  $^{40}\text{Ar}/^{39}\text{Ar}$  and K/Ar ages were determined on sanidine and whole-rock separates of volcanic rocks in the Songliao basin (SB). The volcanism is characterized by a series of continual and episodic eruptions in the late Jurassic (147–157 Ma) and early Cretaceous (113–136 Ma). A fairly accurate chronostratigraphic column was first established based on those data. The volcanic activities happened synchronously with closure of the Mongolia–Okhotsk ocean north to the SB. Structures of the volcanogenic successions are S-dipping or SE-dipping fault blocks coupled with N-dipping or NW-dipping major detachment systems. Distribution of the volcanics, revealed by high-resolution seismic reflections, is neither restricted within nor in agreement with the framework of the overlying sedimentary sequence striking NNE. This new evidence fits the overlap model, proposed in the present paper, that formation of the volcanic successions in the SB is related to the subduction of the Mongolia–Okhotsk plate under the Mongolia–North China block during the Jurassic and early Cretaceous, whereas the overlying sedimentary sequence unconformably on the volcanics is tectonically controlled by the oblique subduction of the Pacific plate under the Eurasian plate since late Aptian. In addition, the coal-bearing epiclastic sediments intercalating the volcanics were deposited at the subduction–quiescence episodes when extensional collapse occurred.

**Keywords** Radioisotopic age · Volcanic rock · Songliao basin · Northeast China · Stratigraphy · Tectonics

### **Introduction**

As the largest oil- and gas-producing basin of China, the Songliao basin (SB; Fig. 1) contributes half of the country's annual petroleum production presently, yielding approximately 55 million tons of crude oil per year. Since the first high-production oil well, called Songji-3 Gusher, was successfully drilled on 27 September 1959, a great deal of exploration work has been done on the basin. By the end of 1990, over 200,000 km seismic reflections had been finished and approximately 30,000 wells had been drilled with an accumulative drill footage of ca. 40 million meters (Wang et al. 1993). Since then, studies have been carried out based on that first-hand information.

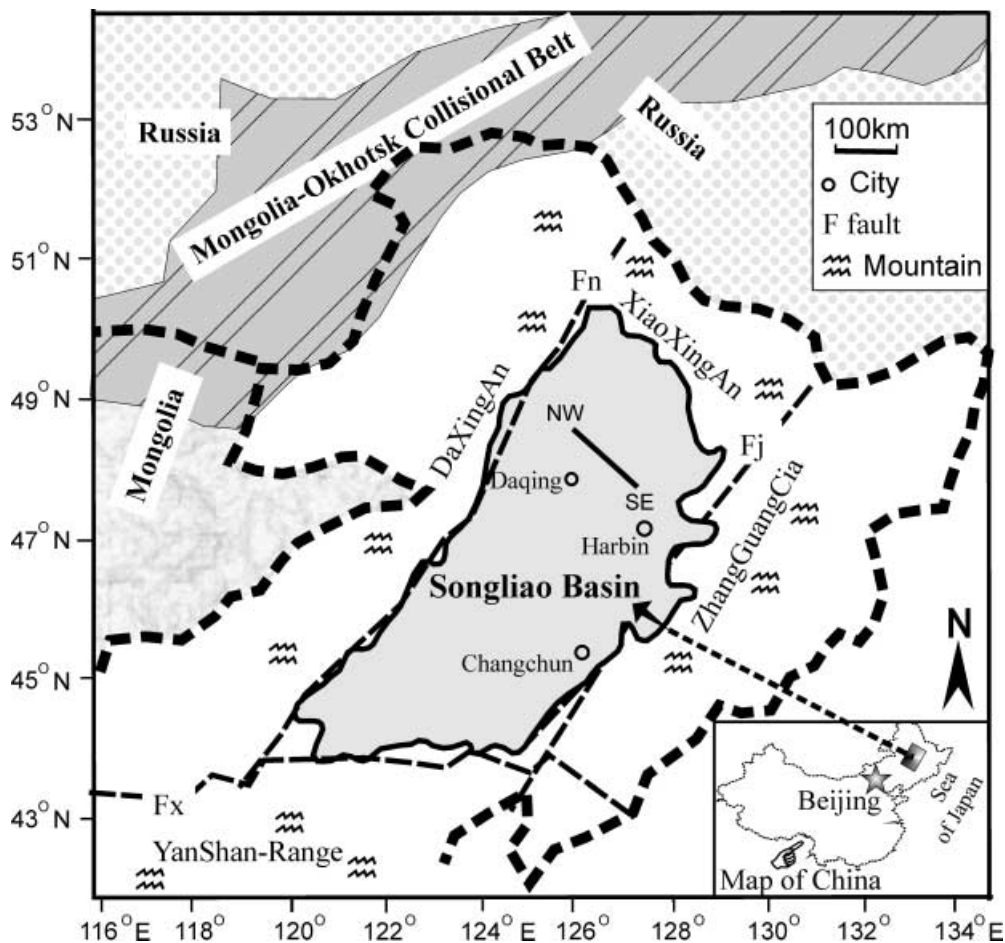
But little attention has been paid to volcanic rocks in the SB until several high-production gas wells were developed in the mid-1990s. By then, the ages were poorly defined chronostratigraphically for the volcanic (lava)-pyroclastic-tuffaceous successions. The corresponding correlation of the volcanogenic units was uncertain. There are mainly three reasons for the poor understanding of the volcanic rocks in the SB despite decades of oil and gas exploration in the area. One reason is the scarcity of fossils in the volcanic sequences. Another reason is the limited availability of drill-hole samples of the deeply buried (>3000 m below the surface) volcanic rocks. The most important reason among them is that they used to be considered as underlying “basement” of the SB and not related to the generation, migration and accumulation of hydrocarbon in the basin.

The newly obtained core sections from drilling and high-quality deep seismic reflections in recent years provide good selection of samples and better understanding of the subsurface structures of the volcanic successions (Shao et al. 1999; Yang et al. 1999; Yang and Wang 1999). The aim of the present study was to get reliable geological ages for the hitherto poorly dated volcanic rocks in the SB and to constrain the temporal and spatial relationship between volcanism and regional tectonic events, thereby recognizing the tectonic environment of emplacement of the volcanic rocks; however, the primary

PJ. Wang (✉) · WZ. Liu · WH. Song  
Earth Sciences' College, JiLin University, JianSheJie Street 79,  
130061 Changchun, Jilin, China  
e-mail: wpjsw@public.cc.jl.cn  
Tel.: +86-431-8584422, Fax: +86-431-8928327

SX. Wang  
Daqing Well-logging (LuJing) Company, 163411 Daqing, China

**Fig. 1** Location of the Songliao basin, NE China, showing related fault belts and mountain ranges



aim and first application of this study was the establishment of the stratigraphic column for the volcanic successions of the SB (Fig. 2), in order to meet the urgent need of petroleum exploration in this area.

### Regional geology

The NNE-striking Songliao basin with a length of ca. 820 km and a width of ca. 350 km (Fig. 1) is a giant nonmarine basin filled with up to 10 km of the Jurassic and Cretaceous sequences. Strata in the basin consist of interlayered volcanic–pyroclastic–epiclastic rocks at its lower part (ca. 250 to >5000 m in thickness; Fig. 2) and sedimentary rocks in the upper part (ca. 4000–6000 m in thickness; Gao 1995; Wang et al. 1996). The basement of the SB is composed of late Palaeozoic low-grade metamorphic/sedimentary rocks (slate, phyllite and carbonate rocks), Hercynian granites and Precambrian schists and gneisses (Fig. 2).

The SB is bounded by fault zones and mountain ranges around (Fig. 1). South of the SB is the Xilamulun suture zone (Fx in Fig. 1) formed in the Permian (Wang and Fan 1997; Zhang et al. 1999). North to the SB is the Mongolia–Okhotsk collisional belt formed during the Jurassic and early Cretaceous because of closure of the

Mongolia–Okhotsk ocean (Scotese et al. 1988; Zhao et al. 1990; Enkin et al. 1992; Zorin 1999). Along the eastern margin of the SB runs the Jiayi fault zone (Fj in Fig. 1) which is the northward extension of the Tanlu fault formed by subduction of the Pacific plate under the Eurasian plate in the late Late Cretaceous and Tertiary (Xu and Ma 1990; Ross et al. 1996). The Mesozoic reactivated Nenjing fault (Fn in Fig. 1) formed its western margin (Sun et al. 1999).

The volcanogenic successions in the SB are stratigraphically bounded by two regional angular unconformities which can be recognized both from seismic reflection in the basin (Shao et al. 1999; Yang and Wang 1999) and on outcrops around the basin (Shan et al. 1999; Wang et al. 1999). They rest unconformably on the underlying basement and are in turn overlain unconformably by the overlying sedimentary sequences (Fig. 2).

### Previously available data of the volcanics/tuffites in the Songliao Basin

By 1996, 27 K/Ar ages of the volcanic rocks in the SB were made available, 14 for the Jurassic andesitic rocks and 13 for the Cretaceous rhyolitic rocks. The samples were collected and analysed unsystematically during the

**Fig. 2** Stratigraphic column of the Jurassic and early Cretaceous volcanogenic successions within the Songliao basin, NE China. Time scale in the left column after Gradstein and Ogg (1996)

Stage	Formation Thickness	Stratigraphic column	Lithologic description	Fossil Assemblage	Age [Ma]
	K1q 400-600m		Laminated multi-coloured pelite, siltstone, and sandstone	<i>Trilobosporites</i> <i>Polyporopollenites</i>	98.9
Albian	K1d 400-600m		Laminated dark colour pelite, siltstone, and sandstone	<i>Schizaeoisporites</i> <i>Classopollis</i> <i>Leiotriletes</i> <i>Polypodiaceasporites</i> <i>Gleicheniidites</i> <i>Clavatipollenites</i> <i>Cyathidites</i> <i>Clavatipollenites</i>	
112.2 Aptian					
	K1yc 100-1200m		Light colour rhyolite, dacite, andesite, basaltic trachyandesite, tephrite; with interbeddings of coarse clastic rocks and coal seams	<i>Macxisporites</i> <i>Verrutritiletes</i> <i>Trileites</i> <i>Ruffordia-Onychiopsis (late sp.)</i> <i>Piceites</i> <i>Piceapollenites</i>	113.19 ± 0.37 (Ar/Ar age)
121.0 Barremian					
127.0 Hauterivian					126.35 ± 0.53 (Ar/Ar age)
132.0 Valanginian	K1yc + K1sh		Lateral alternations of K1yc and K1sh	<i>Granulatisporites</i> <i>Lophotritiletes</i> <i>Ricinospora leavigata</i>	130
137.0 Berriasian	K1sh 150-1150m		Dark colour tuffites, clastic sediments and coal beds	<i>Classopollis</i> <i>Osmundacidites</i> <i>Trileites sp.</i> <i>Macxisporites</i>	135.96 ± 0.28 (Ar/Ar age)
142.0 Tithonian					
150.7 Kimmeridgian	J3hs 0-1000m		Grey andesite, trachyandesite, basaltic trachyandesite, trachyte and rhyolite; with intercalations of fossil-bearing tuffites	<i>Aequitriradites</i> - <i>Cicatricosisporites</i> - <i>Protoconiferus</i>	145.6 147.77 ± 0.28 (Ar/Ar age)
154.1 Oxfordian					
159.4 Calloviaian to Aalenian	J2t-J2b 0-1100m		Dark colour volcanics tuffites and/or siliciclastic sediments	<i>Coniopteris-Phoenicopsis (late sp.)</i>	157.19 ± 0.19 (Ar/Ar age)
Toarcian to Hettangian	J1h 0-600m		Coal-bearing dark siliciclastic sediments	<i>Coniopteris-Phoenicopsis (early sp.)</i>	180.1
Paleozoic and Pre-cambrian basement			Slate, phyllite, carbonate, granite, schist, gneiss		205.7

— conformity; - - - parallel unconformity; angular unconformity; T3-T5 seismic reflector

1970s and 1980s by different workers. These unpublished data were edited by Gao and Xia (1995) and summarized by Wang (1994; Gao and Xiao provided the data in 1991). The data cover a wide age range (Fig. 3), probably due to both inappropriate sampling of altered and xenocryst-bearing rocks and inaccurate analytical technique at that time. As a result of the poor quality, those results were given little attention; thus, the volcanic successions in the SB were classified and correlated lithostratigraphically and biostratigraphically only using

the sedimentary interbeds between the volcanics (Gao 1995; Song et al. 1999). But because of the paucity and low stratigraphic value of the fossils in the non-marine clastic intercalations, the geological ages for the volcanic successions were poorly defined, making it impossible to correlate the volcanic activities in the SB accurately with regional tectonic events.

**Fig. 3** K–Ar age frequency diagram with previously available data for the volcanic rocks in the Songliao basin, NE China. Data from Gao and Xia (1995) and Wang (1994)

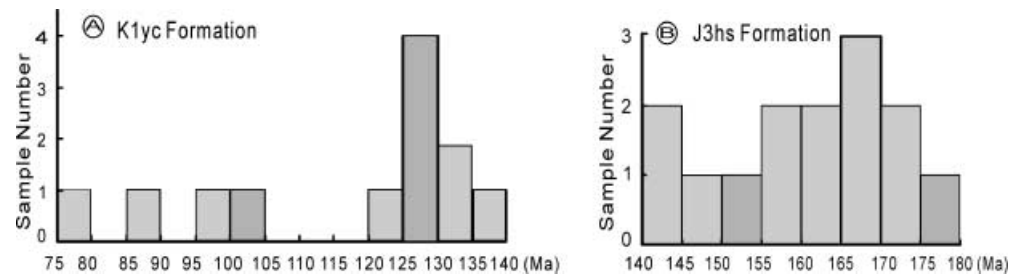


**Table 1** Whole rock K–Ar data of the volcanic rocks in the Songliao basin, NE China

Sample no.	Weight (g)	K <sub>2</sub> O%	Radiogenic <sup>40</sup> Ar*(10 <sup>-10</sup> mole/g)	<sup>40</sup> Ar (rad)%	<sup>40</sup> Ar/ <sup>40</sup> K	Calculated Age ±1SD (Ma)
D279 K	0.1100	4.37	8.026	90.9	0.006000	102.9±1.2
J014	0.04201	3.64	6.948	90.29	0.006378	106.6±1.1
D221	0.1426	3.02	6.012	92.82	0.006670	111.3±1.0
NL-20	0.1700	1.91	3.964	78.95	0.006900	115.9±2.5
Rhyo1 K	0.1523	3.65	8.1242	93.8	0.007478	124.3±4.3
Rhyo1K <sup>a</sup>	0.1731	3.64	7.8867	83.4	0.007259	120.8±5.4
Rhyo2 K	0.1813	4.47	10.241	89.9	0.007676	127.5±5.5
Rhyo3 K	0.1491	4.72	10.497	92.4	0.007451	123.9±5.3
Rhyo3K <sup>a</sup>	0.1684	4.72	10.409	86.7	0.007389	122.9±5.7
Rhyo4 K	0.1604	4.46	10.251	89.8	0.007701	127.9±5.8
Rhyo5 K	0.0613	3.79	8.527	90.1	0.007538	125.3±1.2
Rhyo5K <sup>a</sup>	0.0534	3.79	8.613	88.9	0.007614	126.5±1.3
Rhyo6 K	0.1728	2.93	6.5822	91.2	0.007527	125.1±5.0
Rhyo7 K	0.1567	2.32	5.3724	86.7	0.007759	128.8±5.7
Rhyo9 K	0.0831	4.28	5.069	89.6	0.007450	123.9±1.3
Rhyo10 K	0.0608	3.38	7.738	88.6	0.007670	127.4±1.5
Rhyo11 K	0.0377	2.38	6.013	89	0.008465	140.1±1.9
Rhyo13 K	0.1232	5.78	9.523	93.5	0.008441	139.7±1.5
Daci14 K	0.1784	2.43	5.7035	87.3	0.007864	130.5±5.8
Daci15 K	0.1753	1.49	3.387	87.2	0.007616	126.5±1.4
Trac16 K	0.1889	2.31	5.4878	86.5	0.007959	132.1±5.9
Ande17 K	0.2097	1.05	2.5222	69.5	0.008094	133.5±6.1
Ande18 K	0.1618	3.10	6.9327	86.1	0.007493	124.6±4.6
Ande19 K	0.0689	1.92	4.220	88.4	0.007365	122.5±1.3
BTan20 k	0.1740	1.05	2.4799	66.7	0.007914	131.3±5.9
Teph21 K	0.2437	1.50	3.3954	89.6	0.007583	126.0±5.2
BTan31 K	0.1867	1.31	2.913	86.7	0.007452	123.9±1.3
Rhyo32 K	0.0812	3.02	6.635	94.2	0.007361	122.5±1.0
Daci33 K	0.05015	3.19	7.124	88.7	0.007483	124.4±1.3
Rhyo34 K	0.1343	3.42	7.911	92.9	0.00775	128.7±1.3
BTan35 K	0.2103	1.63	1.469	85.6	0.007811	129.7±1.5
Rhyo22 J	0.0701	3.74	10.47	92.5	0.009381	154.6±2.1
Trac23 J	0.1352	3.57	9.3939	90.0	0.008817	145.7±6.2
Trac24 J	0.1935	2.09	5.9759	86.0	0.009581	157.8±7.3
Tand25 J	0.1564	2.25	5.9784	89.4	0.008903	147.1±6.5
Tand26 J	0.0657	2.48	6.891	89.9	0.009309	153.3±2.3
Ande27 J	0.1335	2.49	6.941	85.5	0.009340	153.9±2.1
Ande27J <sup>a</sup>	0.1311	2.54	7.013	83.9	0.009250	152.6±2.3
Ande28 J	0.0795	1.31	3.710	89.0	0.009489	156.3±2.5
Ande29 J	0.1007	0.67	1.940	86.8	0.009702	157.9±2.7
BTan30 J	0.1426	2.68	7.502	92.2	0.009379	154.6±2.2

Whole rock K–Ar data measured in Beijing Geological Institute of Chinese Academy with RGA-10 gas mass spectrometer of British VSS Company, using the constants recommended by Steiger and Jaeger (1977)  
<sup>a</sup> The second results of the same sample obtained by secondary determination in the same laboratory 1 year after the first analysis

### Sampling and analytical techniques

The volcanic rocks were recovered from the depths between 1500 and 4800 m below the surface within the SB. More than 300 volcanic samples were collected from the selected core sections for this study. Thin-section work was done on all the samples. The volcanics are fine grained, porphyric texture, with phenocrysts of quartz, plagioclase, sanidine, biotite, hornblende, pyroxene and

spinel, and with the groundmass minerals compositionally similar to the phenocrysts. The phenocrysts are 0.5–2.5 mm in length, and 5–20% in volume percent. Xenoliths and xenocrysts were recognized in the upper Jurassic volcanic rocks during regional geological survey and microscope investigation. Secondary alterations were locally observed on the scales both of outcrop and microscope, including calcitization, silica/chabazite or analcite fillings. We chose samples without observable

**Table 2** Bulk chemical composition of the volcanic rocks in the Songliao basin, NE China

Sample	SiO <sub>2</sub>	CaO	MgO	Al <sub>2</sub> O <sub>3</sub>	P <sub>2</sub> O <sub>5</sub>	MnO	FeO	TFeO	TiO <sub>2</sub>	Na <sub>2</sub> O	K <sub>2</sub> O
Rhyo1 K	77.78	0.65	0.22	11.12	0.03	0.01	1.17	2.04	0.13	3.95	3.75
Rhyo2 K	77.39	0.25	0.44	12.02	0.04	0.02	0.73	1.43	0.17	3.33	5.06
Rhyo3 K	80.08	0.40	0.97	10.91	0.04	0.04	1.19	2.00	0.10	0.35	5.25
Rhyo4 K	75.22	0.51	1.30	14.20	0.04	0.03	0.77	1.59	0.08	1.76	4.92
Rhyo5 K	82.70	0.05	0.76	9.33	0.03	0.04	0.13	0.99	0.04	3.66	3.14
Rhyo6 K	75.89	0.366	0.72	13.39	0.04	0.03	0.32	2.05	0.14	4.26	3.53
Rhyo7 K	82.38	0.29	0.33	10.06	0.04	0.01	0.92	2.06	0.13	1.63	2.64
Rhyo8 K	82.32	0.22	0.44	9.30	0.03	0.03	0.61	0.99	0.04	2.23	4.24
Rhyo9 K	75.60	0.44	0.59	12.03	0.04	0.04	1.94	2.96	0.16	3.12	4.96
Rhyo10 K	76.52	0.56	0.60	12.07	0.04	0.03	0.27	2.58	0.04	4.50	3.01
Rhyo11 K	78.30	0.74	0.13	12.95	0.00	0.06	0.54	0.78	0.12	4.54	3.08
Rhyo12 K	75.75	0.40	0.28	12.84	0.03	0.03	1.44	2.55	0.17	3.65	4.82
Rhyo13 K	82.80	0.11	0.06	9.67	0.05	0.01	0.60	0.69	0.13	1.19	5.89
Daci14 K	75.56	0.35	3.93	11.27	0.03	0.05	1.26	4.48	0.11	0.93	2.89
Daci15 K	77.68	0.85	0.89	14.40	0.01	0.01	1.05	0.95	1.76	0.14	1.54
Trac16 K	65.60	1.10	4.74	16.87	0.05	0.08	1.49	3.77	0.58	4.65	2.67
Ande17 K	63.16	0.41	4.47	16.57	0.06	0.23	1.78	7.66	1.45	5.12	1.41
Ande18 K	65.51	1.07	3.66	16.78	0.05	0.08	3.70	5.53	0.92	2.51	3.46
Ande19 K	63.57	2.74	5.98	13.90	0.05	0.22	3.11	9.15	1.51	0.54	1.83
BTan20 k	55.96	7.26	4.92	18.06	0.05	0.13	3.58	6.92	0.91	4.21	1.56
Teph21 K	54.43	1.12	3.93	16.07	0.07	0.22	3.54	12.01	3.53	6.48	1.84
BTan31 K	55.60	5.00	1.62	22.64	0.01	0.38	6.30	6.16	2.05	4.04	1.78
Rhyo32 K	72.53	2.15	0.28	14.50	0.05	0.06	2.06	2.26	0.76	3.43	3.24
Daci33 K	66.83	2.73	0.71	13.48	0.17	0.13	9.75	9.19	1.66	2.85	1.45
Rhyo34 K	82.48	0.03	0.20	9.24	0.03	0.04	0.97	1.29	0.10	2.60	3.76
BTan35 K	55.76	6.86	2.04	17.52	0.10	0.11	6.49	8.40	1.96	4.58	1.55
Rhyo22 J	77.65	1.08	0.64	11.51	0.07	0.06	0.68	2.34	0.28	1.85	4.52
Trac23 J	67.84	1.48	3.10	14.92	0.04	0.04	1.75	2.94	0.45	4.62	4.12
Trac24 J	67.58	2.00	1.91	16.36	0.04	0.051	2.02	3.06	0.42	5.99	2.23
Tand25 J	63.24	3.15	4.17	16.38	0.04	0.09	2.76	4.31	0.58	4.96	2.58
Tand26 J	64.67	4.95	2.00	16.80	0.21	0.11	0.48	3.86	0.67	4.66	2.80
Ande27 J	65.23	4.49	0.57	18.51	0.37	0.12	0.60	3.77	0.71	4.53	2.62
Ande28 J	61.80	5.43	3.70	16.78	0.19	0.11	1.34	6.26	0.81	4.861	1.41
Ande29 J	64.72	4.06	3.56	16.42	0.19	0.06	2.04	5.41	0.77	5.05	0.82
BTan30 J	55.92	8.69	4.02	16.97	0.32	0.12	1.35	7.08	1.15	4.17	1.65

alterations and xenocrysts from the suite for radioisotopic dating. Special care was taken to exclude joint and cleavage surfaces, and veinlets from the samples. All the envisaged samples were smashed into 25 to 60 mesh, and this was expected to help exclude the potential altered materials from the samples because the altered ones are in general friable. Single crystals of sanidine, obtained by hand-picking under binocular microscope, were used for <sup>40</sup>Ar/<sup>39</sup>Ar dating. The sanidine grains were selectively checked with electron-beam microscope (JEM-2000FX) and analysed with the attached energy-dispersive spectrometer (TN-5500). They were proved to be fresh enough without recognizable alterations (e.g. K<sub>2</sub>O%=14–17). Whole rocks were used for K/Ar analysis (Table 1). All the sample grains were checked with microscope before isotopic determination. Chemical compositions were determined before radioisotopic analysis (see Table 2).

The <sup>40</sup>Ar/<sup>39</sup>Ar step-heating and K/Ar isotope dilution analyses were performed on the volcanics including rhyolite, dacite, trachyte, andesite, trachy-andesite, basaltic-trachyandesite and tephrite, at the Geological Institute of Chinese Academy, Beijing, using the procedures described by Sang et al. (1997). See notes to Table 3 for irradiation monitors and other basic related information.

### K/Ar results compared with previous data

The K/Ar results are presented in Fig. 4 and Table 1. The apparent ages for the lower Cretaceous volcanics (called Yingcheng Formation, abbreviation K1yc) range 102.9–140.1 Ma with analytical errors of 1.0–6.1 Ma. Those of the upper Jurassic (Huoshiling Formation, J<sub>3</sub>hs) are 145–160 Ma with analytical errors of 2.1–7.3 Ma. Compared with the previously available data in Fig. 3, the newly determined results are less dispersed and give continuous age spectra. The ages below 100 Ma are missing in the new results (Fig. 4A), although the former group of samples is stratigraphically included in the new one. We believe that this is because the new samples are fresh enough to eliminate the possibility of argon loss caused by alteration, since we have much more choice of samples than ever before with the newly drilled wells. There are no ages over 160 Ma in Fig. 4B with respect to the previous ages in Fig. 3B. One possibility resulting in the abnormally former ages for the previous data is xenocrystal (even xenolithic) contamination, because some of the xenoliths are bigger than the diameter of core section, making it possible to use xenoliths as analysed specimen. But we could not re-analyse the former samples for checking because they had been used. Despite the

**Fig. 4** K–Ar age frequency diagram with recently determined data for the volcanic rocks in the Songliao basin, NE China (data from Table 1).

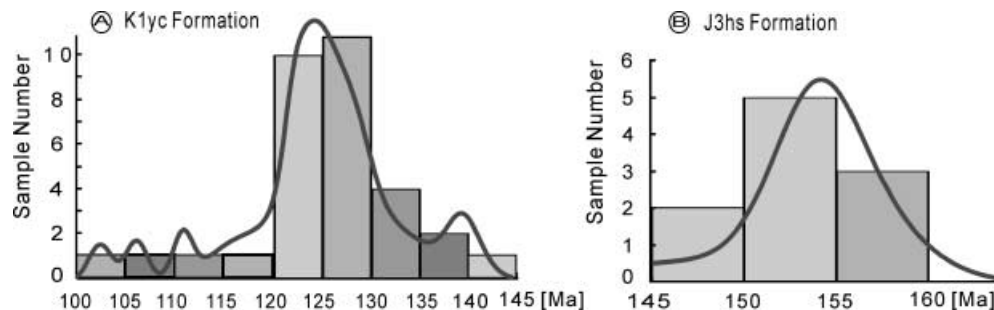


**Table 3** Criteria of  $^{40}\text{Ar}/^{39}\text{Ar}$  results corresponding to the plots in Fig. 5

Sample no. and formation	NL-20 Top of K1yc	Rhyo13 K Base of K1yc	Kq-31 Middle of K1yc	Tand25 J Top of J3hs	Ande29 J Base of J3hs
Material	Sanidine	Sanidine	Sanidine	Sanidine	Sanidine
$N_{\text{plateau}}$ and $^{39}\text{Ar}$ fraction	7 (97%)	7 (95%)	7 (93%)	7 (95%)	7 (94%)
Plateau age $\pm 2\sigma$ (Ma)	113.2 $\pm$ 0.4	136.0 $\pm$ 0.3	126.4 $\pm$ 0.5	147.8 $\pm$ 0.3	157.2 $\pm$ 0.2
Inverse isochron age $\pm 2\sigma$ (Ma)	114.2 $\pm$ 3.8	136.2 $\pm$ 6.4	127.1 $\pm$ 3.6	148.4 $\pm$ 8.3	157.8 $\pm$ 9.2
$(^{40}\text{Ar}/^{36}\text{Ar})_0 \pm 2\sigma$	290.0 $\pm$ 16.0	295.0 $\pm$ 13.0	291.0 $\pm$ 31.0	293.0 $\pm$ 13.0	293.0 $\pm$ 15.0
MSWD	0.4	0.3	2.9	0.2	0.1
$(^{37}\text{Ar}/^{39}\text{Ar})_m \pm \sigma$	0.0812 $\pm$ 0.0451	0.0970 $\pm$ 0.0530	0.1680 $\pm$ 0.1571	0.0575 $\pm$ 0.0268	0.0408 $\pm$ 0.0286
Mean K/Ar age $\pm 2\sigma$ (Ma)	115.9 $\pm$ 5.0	139.7 $\pm$ 3.0	no data	147.1 $\pm$ 13.0	157.9 $\pm$ 5.4

Samples were irradiated for 51.5 h in the neutron nuclear reactor at Atomic Energy Institute of China. Sample grains were step heated using a radio frequency furnace. Samples and standards were put in the same irradiation ampoule of 40 mm in diameter and 45 mm in height that rotates during irradiation. Instantaneous fast neutron flux is  $3.44 \times 10^{12} \text{ n/cm}^2 \text{ s}^{-1}$ , integrated fast neutron flux is  $6.38 \times 10^{17} \text{ n/cm}^2$ . Samples have 60–80%  $^{40}\text{Ar}^*$ . The monitor standards, located about every two samples, were sanidine of America FCT-1 (27.5 $\pm$ 0.2 Ma), biotite of Australia GA1550

(97.9 $\pm$ 0.7 Ma), hornblende of China ZBJ (132.8 $\pm$ 1.4 Ma), biotite of China ZBH-25 (132.7 $\pm$ 1.2 Ma) and hornblende of international standard BSP-1 (2026 $\pm$ 8 Ma). Ages were calculated using the constants:  $\lambda = 5.543 \times 10^{-10} \text{ year}^{-1}$ ;  $\lambda_e = 0.581 \times 10^{-10} \text{ year}^{-1}$ ; and  $J = 0.01219 \pm 0.00012$ . Abundances of five Ar isotopes were measured. The correction factors are  $(^{40}\text{Ar}/^{36}\text{Ar})_a = 294.2 \pm 3\%$ ,  $(^{36}\text{Ar}/^{37}\text{Ar})_{Ca} = 2.64 \times 10^{-4} \pm 2\%$ ,  $(^{40}\text{Ar}/^{39}\text{Ar})_K = 3.05 \times 10^{-2} \pm 1\%$  and  $(^{39}\text{Ar}/^{37}\text{Ar})_{Ca} = 6.87 \times 10^{-4} \pm 2\%$ . Raw data of  $^{40}\text{Ar}/^{39}\text{Ar}$  can be obtained by the authors on request

differences mentioned previously, there are general agreements between the previous data (Fig. 3) and the new ages (Fig. 4). For example, the age frequency peaks of 120–135 Ma are in Figs. 3A and 4A, and the overlapping of 145–160 Ma exists in between Figs. 3B and 4B.

The big problem of the obtained K/Ar ages is the continuous age distribution from 100 to 160 Ma (Fig. 4). There must be a time hiatus because there is a sedimentary sequence up to 1150 m thick in between the two volcanic formations (i.e. K1sh in Fig. 2). In order to solve this problem,  $^{40}\text{Ar}/^{39}\text{Ar}$  dating was done.

#### $^{40}\text{Ar}/^{39}\text{Ar}$ results and constraints on K/Ar ages

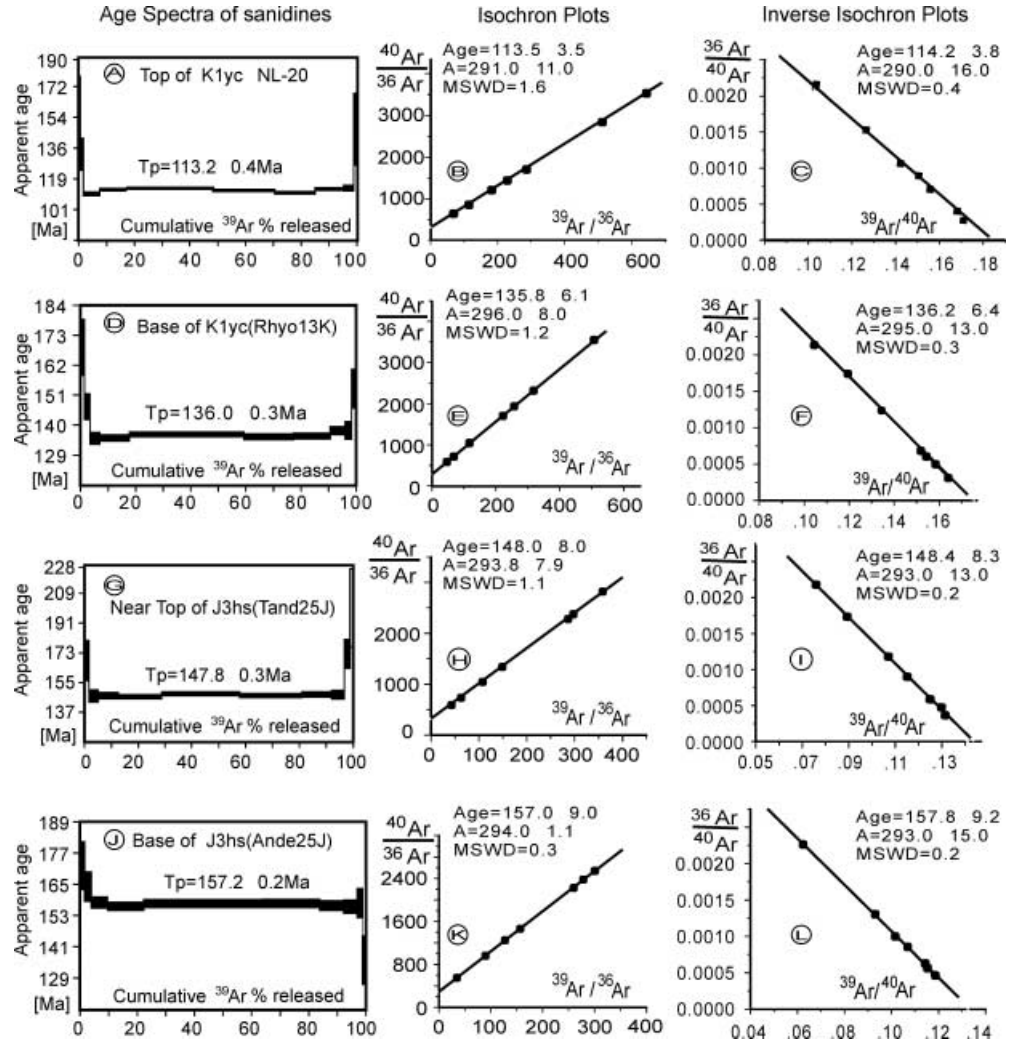
Four sets of  $^{40}\text{Ar}/^{39}\text{Ar}$  samples were selected from the top and bottom boundaries of the two volcanic formations (Figs. 2, 5). In addition, a sample equivalent to the middle K<sub>1</sub>yc volcanics gave a  $^{40}\text{Ar}/^{39}\text{Ar}$  plateau age of 126 Ma (Fig. 2); therefore, the Lower Cretaceous volcanics (K<sub>1</sub>yc) are confined to 113–135 Ma, and the Upper Jurassic (J<sub>3</sub>hs) to 147–157 Ma, indicating a time interval of ca. 12 Ma in between the two volcanogenic formations (Fig. 2).

We chose to present the data on isotope correlation and inverse isotope correlation diagrams because this

method allows simple visualization of the age, initial trapped argon component ( $^{40}\text{Ar}/^{36}\text{Ar}$ ) and xenocrystic contamination (Miller et al. 1998). Ten heating steps were used in analysing the samples in Fig. 5. The initial two and the last steps gave relatively older ages, whereas the remaining seven steps show a plateau age with  $^{39}\text{Ar}$  release over 94% (Table 3), typically showing rough U- or saddle-shaped release patterns. The initial  $^{40}\text{Ar}/^{36}\text{Ar}$  ratios given by the y-intercepts are within the analytical error of the atmospheric value (295.5). The sample at the base of J<sub>3</sub>hs formation (Figs. 5J–L) is different from the three others in that it has abnormally low age at the last incremental-heating step.

A rigorous criterion for a plateau age is the identification of series of adjacent steps which together comprise more than 50% of the total argon release, each of which yields an age within 2 standard deviations of the mean (Dickin 1995). Sinton et al. (1998) defined a reliable age, namely the crystallization or cooling age, with three criteria: (a) a well-defined age spectrum plateau of at least three concordant consecutive steps that represents at least 50% of the total  $^{39}\text{Ar}$  release; (b) a concordant isochron age in which the F-distribution statistic SUMS/(N-2) is below the cut-off value at 95% confidence level; and (c) the  $^{40}\text{Ar}/^{36}\text{Ar}$  intercept is statistically

**Fig. 5A–L** Flat release age spectrum (left), corresponding isochron plot (middle) and inverse isochron plot (right) for the volcanic rocks in the Songliao basin, NE China. A=y-axis intercept (initial  $^{40}\text{Ar}/^{36}\text{Ar}$ ); MSWD mean square of weighted deviates; J=irradiation parameter ( $0.01219\pm 0.00012$ ) obtained from standard



indistinguishable (within 1 s) from the atmospheric value 295.5. The key criteria of the  $^{40}\text{Ar}/^{39}\text{Ar}$  results in Fig. 5 are listed in Table 3. In comparison with the discrimination criteria, the authors interpret the  $^{40}\text{Ar}/^{39}\text{Ar}$  results in Fig. 5 as the hitherto best approach to cooling ages of the volcanic rocks within the SB.

### Radioisotopic dating constraints on stratigraphy

The two volcanic formations of J<sub>3</sub>hs and K<sub>1</sub>yc are intercalated by the coal-bearing siliciclastic rocks with minor tuffites, called Lower Cretaceous Shahezhi Formation (K<sub>1</sub>sh Form.). It represents fluvial and lacustrine facies. Intercalated in the volcanics of K<sub>1</sub>yc are coal-bearing clastic deposits with alluvial-braided stream facies. There are several interbeds of fossil-bearing tuffites in the J<sub>3</sub>hs volcanic rocks, too. It was the fossil assemblages contained in those sedimentary units that allowed establishment of a rough regional stratigraphy adjacent to the studied area during the geological mapping of 1:200,000 in the 1960s and 1970s (Wang et al. 1996). With the same procedure coupled with geophysical methods, the strati-

graphic section for the volcanics within the SB was set up in the late 1990s. That kind of correlation can confine the age of the volcanics in the SB to the Middle and Late Mesozoic (Gao 1995; Shan et al. 1999; Song et al. 1999).

Our  $^{40}\text{Ar}/^{39}\text{Ar}$  ages of the volcanic rocks in the SB provided five fairly precise chronostratigraphic points (Fig. 2); thus, we propose the correlation with European stages (Gradstein and Ogg 1996) for the volcanogenic successions in the SB (Fig. 2).

### Radioisotopic dating constraints on basin dynamics

The Mesozoic volcanic activities in the SB happened in the late Jurassic of 147–157 Ma and early Cretaceous of 113–135 Ma (Fig. 2). They seem to be characterized by a series of continual coupled with intensively episodic eruptions according to radioisotopic data and field observations. In the meantime and afterwards, several prominent regional tectonic events occurred in the region. Among these events were:

1. Closure of the Mongolia–Okhotsk ocean north to the SB (cf. Fig. 1). This resulted in the corresponding

**Fig. 6** Subsurface stratigraphic and structural section of line NW–SE in Fig. 1

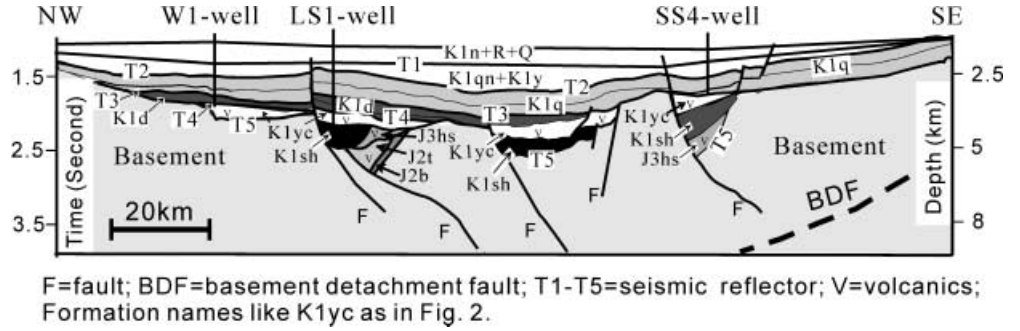
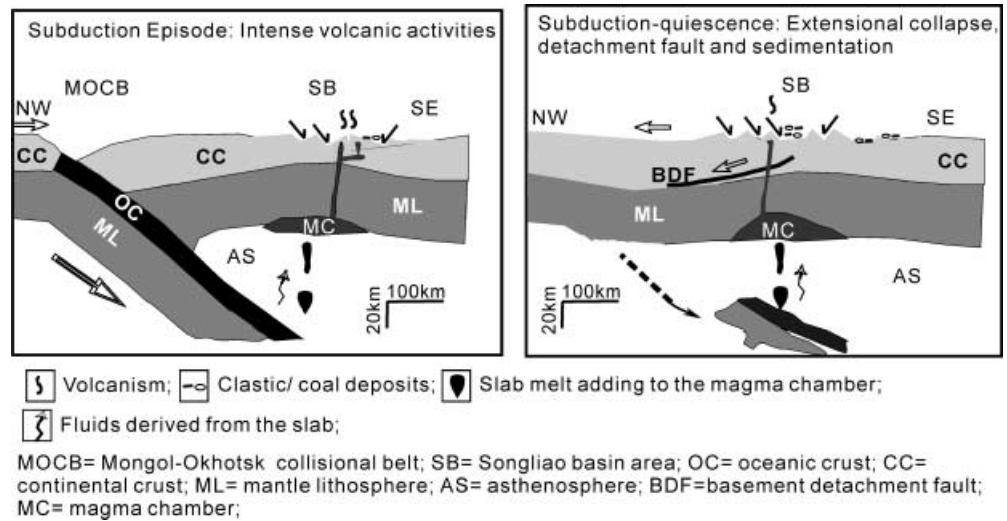


**Fig. 7** Schematic model for the Late Jurassic and Early Cretaceous geodynamics of the Songliao basin, NE China



- Mongolia–Okhotsk collisional belt during 155–95 Ma (Scotese 1997 Internet maps; related publication in Scotese et al. 1988; Zhao et al. 1990; Enkin et al. 1992; Zorin 1999).
2. Regional deformation events on the NE Asian continental margin in 134–92 and 70–30 Ma, corresponding to assumed proto-Pacific plate motions (Khudoley and Sokolov 1998).
  3. Igneous activities along East Asia continental margin ascribed to the subduction of proto-Pacific plates (preferably called Farallon-Izanagi and Kula-Pacific ridges here). This magmatism was dated 95–65 Ma and was observed in SW Japan, 1000–1500 km east of the SB (Kinoshita 1995).
  4. Opening of the Japan Sea during 23–15 Ma resulted from backarc spreading (Yamaji 1990; Lee et al. 1999).

The present outline of the SB is the relict after the regional tectonic movement during the late Late Cretaceous and Tertiary because of the oblique subduction of the Pacific plate under the Eurasia plate along NE Asia continental margin (approximately equivalent to the deformation episode of 70–30 Ma of Khudoley and Sokolov 1998). This event, which may have lasted until 15 Ma from the late Late Cretaceous, was so influential to the SB. It resulted in the uplift and erosion of the eastern part of the basin, obscured all former structures and

finally gave the SB its present outline of NNE strike (Fig. 1). As a result, angular unconformities and inverse structures were formed during this period (Gao 1995; Wang et al. 1996; Song 1997). As a result, it has long been believed that the movement of the Pacific plate (east to the SB) was the predominant dynamic throughout the whole evolution of the basin (Liu et al. 1993; Sun et al. 2000).

However, the distribution of the volcanic successions is neither restricted within nor in agreement with the framework of the overlying sedimentary sequence of NNE-strike (represented by the present basin shape shown in Fig. 1). For example, it has been found, by geological survey and geophysical data in the past 3 years, that the thickest succession of the volcanics developed on the southeastern edge, instead of in the centre of the SB (Wang et al. 1999; Yang and Wang 1999). Structures of the volcanic successions, revealed by high-resolution seismic reflection of 1998, are obviously different from those of the overlying sequence, too. They show prevalingly S-dipping or SE-dipping fault blocks coupled with predominantly N-dipping or NW-dipping major detachment systems (Fig. 6; Yang et al. 1999). On the other hand, the radioisotopic results of the volcanics in the paper indicate closely temporal affinity of the volcanisms in the SB (113–135 and 147–157 Ma) to the activities of the Mongolia–Okhotsk belt (155–95 Ma). In contrast, significant igneous activities related to the

subduction of the Pacific plate occurred during 95–65 Ma in the region (Kinoshita 1995), later than the volcanisms in the SB. Moreover, the Pacific plate-controlled tectonic event of 134–92 Ma in the near-Pacific part of the region is characterized by imbricate fans of thrusts and folds with southeast vergence, broken formation and serpentinite melange (Khudoley and Sokolov 1998), which can hardly compare with the features of the synchronous SB. In addition, the Mongolia–Okhotsk collisional belt is the nearest possible element to the SB in the area.

To fit the new evidence given above, the authors proposed an overlap model to explain the dynamics of the SB: namely, accompanied by opening of the basin, the volcanic successions in the SB are related to the subduction of the Mongolia–Okhotsk plate under the Mongolia–North China block during the Jurassic and early Cretaceous (Fig. 7), whereas the overlying sedimentary sequence resting unconformably on the volcanics is tectonically controlled by the oblique subduction of the Pacific plate under the Eurasian plate since mid-Cretaceous (e.g. Liu et al. 1993; Dou 1997; Zhang et al. 1999; Sun et al. 2000). This means that the Songliao basin is just a kind of overlap basin with two super-sequences, the volcano-genic succession at its lower part and the overlying sedimentary sequence at its upper part. According to the couplet features between basement detachment systems and the corresponding extensional normal faults as shown in Fig. 6, the coal-bearing epiclastic sediments intercalated in the volcanics were explained to be deposited at the subduction–quiescence episodes when extensional collapse occurred (Fig. 7). There was a transformation of tectonic regime in the region from the Mongolia–Okhotsk (in the north, before Aptian) to the circum-Pacific (in the southeast, after Aptian). It is noted, however, that in order to clarify the genetic dynamics making the giant non-marine Songliao basin, we need more detailed information, such as palaeomagnetic and plate reconstruction, although the precise dating on the volcanics has given some approach to the solution.

## Conclusion

Precise  $^{40}\text{Ar}/^{39}\text{Ar}$  ages coupled with K/Ar results, dated on minerals or whole rock, confined the Cretaceous acidic volcanic rocks to 113–136 Ma, and the intermediate volcanics to 147–157 Ma, respectively, in the Songliao basin (SB). A fairly precise chronostratigraphic column was first established based on those data. Among all the synchronously occurring regional tectonic events, development of the volcanic successions in the SB (157–113 Ma) shows closest time and space affinity with closure of the Mongolia–Okhotsk ocean during 155–95 Ma, suggesting possible dynamic contribution from the north of the SB. This temporal association is further supported by the structure styles of the volcano-genic successions in the SB. They show obviously couplet features, i.e. S-dipping or SE-dipping fault blocks

are accompanied by N-dipping or NW-dipping major detachment systems, implying northwards extensional collapse. Thus, an overlap basin dynamics is proposed, i.e. the volcanic rocks in the SB are related to the subduction of the Mongolia–Okhotsk oceanic plate, whereas its overlying sedimentary sequence belongs to the circum-Pacific tectonic regime. In addition, the coal-bearing epiclastic sediments intercalated in the volcanics were deposited at the subduction–quiescence episodes when extensional collapse occurred.

**Acknowledgements** PJ. Wang is grateful to his German host professors, G. Einsele and M. Satir, and the director of his host institute, P. Grathwohl, for their kind help with the research. Special thanks to L. YouMing and L. Hong, directors of the project (NSFC49894190) “Non-Marine Petroleum Pool Geophysics and 3D Subsurface Mapping”, for their kind advice related to the research. PJ. Wang is indebted to F. Chen for his assistance with computer work, and to Y.-P. Wang for her correction of English. We thank Drs. Kraml and Schneider for their constructive comments on the manuscript. The Isoplot program used in the paper was kindly provided by K. Ludwig through Internet. This work was financially supported by the Natural Science Foundation of China (project nos. 49672124 and 49894190–13) and attained with the assistance of the Alexander von Humboldt Foundation, Germany.

## References

- Dickin AP (1995) Radiogenic isotope geology. Cambridge University Press, London, pp 1–452
- Dou LiRong (1997) The lower Cretaceous petroleum system in NE China. *J Petrol Geol* 20:475–488
- Enkin RJ, Yang ZhenYu, Chen Yan, Courtillot V (1992) Paleomagnetic constrains on the geodynamic history of the major blocks of China from the Permian to the Present. *J Geophys Res* 97:953–989
- Gao RiQi (1995) Petroleum stratigraphy of the Songliao basin. Heilongjiang Science and Technology Press, Haerbin, pp 18–28 (in Chinese)
- Gao RiQi, Xiao DeMing (1995) Proceedings in petroleum exploration and development of Daqing oil field. Petroleum Press, Beijing, pp 14–16 (in Chinese)
- Gradstein F, Ogg J (1996) Geological time scale. Episodes 19:3–5
- Khudoley AK, Sokolov SD (1998) Structural evolution of the northeast Asia continental margin: an example from the western Koryak fold and thrust belt (northeast Russia). *Geol Mag* 135:311–330
- Kinoshita O (1995) Migration of igneous activities related to ridge subduction in Southwest Japan and the East Asian continental margin from the Mesozoic to the Paleogene. *Tectonophysics* 245:25–35
- Lee YS, Ishikawa N, Kim WK (1999) Paleomagnetism of Tertiary rocks on the Korea Peninsula: tectonic implications for the opening of the East Sea (Sea of Japan). *Tectonophysics* 304: 131–149
- Liu ZhaoJun, Wang DongPo, Liu Li, Liu WangZhu, Wang PuJun, Du XiaoDi, Yang Guang (1993) Sedimentary characteristics of the Cretaceous Songliao basin. *Acta Geol Sinica* (English edition) 6:167–180
- Miller JS, Heizler MT, Miller CF (1998) Timing of magmatism, basin formation, and timing at the west edge of the Colorado river extensional corrido: result from single-crystal  $^{40}\text{Ar}/^{36}\text{Ar}$  geochronology of Tertiary rocks in the Old Women mountains areas, southeastern California. *J Geol* 106:195–209
- Ross VR, Mercier J-CC, Xu YiGang (1996) Diffusion creep in the upper mantle: an example from the Tanlu Fault, northeast China. *Tectonophysics* 261:315–329

- Sang HaiQing, Wang SongShan, Hu ShiLing, Qui Ji (1997)  $^{40}\text{Ar}/^{39}\text{Ar}$  dating method and Ar isotopic mass spectrometry analysis of quartz. *J Chinese Mass Spectr Soc* 15:17–27
- Scotese CR, Gahagan L, Larson RL (1988) Plate tectonic reconstruction of the Cretaceous and Cenozoic ocean basins. *Tectonophysics* 155:27–48
- Shan XuanLong, Wang PuJun, Chen ShuMin, Ren YangGuang, Wan Chuan-Biao (1999) Stratigraphy correlation and tectonic signification on Upper Jurassic and Early Cretaceous in the Songliao Basin. *J Changchun Uni Sci Tech Spec Issue* 29: 8–13 (in Chinese with English abstract)
- Shao ZhengQui, Meng XiangLu, Wang HongYan, Wang PuJun (1999) Seismic reflection and distribution of the Late Jurassic–Early Cretaceous volcanic rocks in the Songliao Basin. *J Changchun Uni Sci Tech* 29:30–40 (in Chinese with English abstract)
- Sinton CW, Hitchen K, Duncan RA (1998)  $^{40}\text{Ar}$ – $^{39}\text{Ar}$  geochronology of silicic and basaltic volcanic rocks on the margins of the North Atlantic. *Geol Mag* 132:161–170
- Song TingGuang (1997) Inversion styles in the Songliao basin (northeast china) and estimation of the degree of inversion. *Tectonophysics* 283:173–188
- Song WeiHai, Wan ChuanBiao, Bian WeiHua, Shan XuanLong, Wang PuJun (1999) Biostratigraphy and stratigraphic correlation from Jurassic to Early Cretaceous in the Songliao basin and adjacent areas. *J Changchun Uni Sci Tech Spec Issue* 29:62–69 (in Chinese with English abstract)
- Steiger RH, Jager E (1977) IUGS Subcommittee on Geochronology: convention on the use of decay constants in geo- and cosmochronology. *Earth Planet Sci Lett* 36:359–362
- Sun XiaoMeng, Zhang MeiSheng, Liu Cai, Peng XiangDong (1999) The features and research significance of the Nenjiang fault. *J Changchun Uni Sci Tech Spec Issue* 29:79–82 (in Chinese with English abstract)
- Sun XiaoMeng, Zhang MeiSheng, Yang BaoJun, Zhu DeFeng, Wan CuanBiao (2000) Geological and geophysical features and their structural evolution in Songliao basin. *J Changchun Uni Sci Tech Spec Issue* 30:8–13 (in Chinese with English abstract)
- Wang PuJun (1994) Lake-marine linking events and global correlation of the Songliao nearshore continental basin, Cretaceous, Northeast China. PhD thesis of Changchun Univ Earth Sci, pp 1–145 (in Chinese with 18 pages of English abstract)
- Wang PuJun, Du XiaoDi, Wang Jun, Wang DongPo (1996) Chronostratigraphy and stratigraphic classification of the Cretaceous of the Songliao basin. *Acta Geol Sinica* (English edition) 9:207–217
- Wang PuJun, Wang ShuXue, Qu YongBao, Ren YanGuang (1999) Volcanic events of the Cretaceous Songliao basin: a case study of Yingcheng Formation. *J Changchun Uni Sci Tech Spec Issue* 29:50–55 (in Chinese with English abstract)
- Wang QinYou, Su YangZheng, Liu ErYi (1996) Regional stratigraphy of NE China. China University of Geosciences, Wuhan, pp 1–318
- Wang YuJing, Fan ZhiYong (1997) Discovery of Permian radiolarians in ophiolite belt on northern side of Xilamulun river, Nei Monggu, and its geological significance. *Acta Palaeontol Sinica* 36:58–69
- Wang ZhiWu, Yang JiLiang, Gao RiQi (1993) Petroleum geology of Daqing oil field, 3rd edn. Petroleum Industry Press, Beijing, pp 8–16 (in Chinese)
- Xu JiaWei, Ma GuoFeng (1990) Review of ten years (1981–1991) of research on the Tancheng-Lujiang fault zone. *Geol Rev* 38:316–322 (in Chinese with English abstract)
- Yamaji A (1990) Rapid intra-arc rifting in Miocene Northeast Japan. *Tectonics* 9:365–378
- Yang BaoJun, Wang PuJun (1999) Study on  $T_3$ ,  $T_4$  and  $T_5$  seismic reflection and their geological significance in the Songliao Basin. *J Changchun Uni Sci Tech Spec Issue* 29:13–20 (in Chinese with English abstract)
- Yang BaoJun, Liu Cai, Jiao XinHua, Tang JianRen, Li ChengLi, Liu GuoXing, Yang PingHua (1999) Discussion about the geophysical characteristics of Songliao basin basement. *J Changchun Uni Sci Tech Spec Issue* 29:13–19 (in Chinese with English abstract)
- Zhang MeiSheng, Sun XiaoMeng, Peng XiangDong, Zhang SongMei (1999) Mesozoic tectonic stages of the Songliao basin and adjacent regions. *J Changchun Uni Sci Tech Spec Issue* 29:20–24 (in Chinese with English abstract)
- Zhao XiXi, Coe RS, Zhou YaoXiu, Wu HaoRuo, Wang Jie (1990) New paleomagnetic results from northern China: collision and suturing with Siberia and Kazakhstan. *Tectonophysics* 181: 43–81
- Zorin YA (1999) Geodynamics of the western part of the Mongolia–Okhotsk collisional belt, Trans-Baikal region (Russia) and Mongolia. *Tectonophysics* 306:33–56